Open access • Journal Article • DOI:10.1007/S10652-015-9430-3

Modelling nature-like fishway flow around unsubmerged obstacles using a 2D shallow water model — Source link

Tien Dung Tran, Jacques Chorda, Pascale Laurens, Ludovic Cassan

Published on: 01 Apr 2016 - Environmental Fluid Mechanics (Springer Netherlands)

Topics: Shallow water equations

Modelling nature-like fishway flow around unsubmerged obstacles using a 2D shallow water model

Tien Dung Tran[1] · Jacques Chorda[2] · Pascale Laurens[2] · Ludovic Cassan[2]

Abstract In the scope to create efficient nature like fish ramps using large-scale roughness elements, the present study is an audit of modelling such complex 3D free surface flows using an industrial 2D code solving shallow water equations. Validation procedure is based upon the comparison between numerous experimental measurements and numerical runs around large-scale roughness patterns disposed on the flume bottom in order to determine what 2D reliable numerical results can be expected. In this paper, we focused on cases of unsubmerged obstacles. The results demonstrate that 2D shallow water modelling using an industrial code such as TELEMAC-2D can be a convenient way for the hydraulic engineer to help design a nature-like fishway. This article emphasizes the limitations due to 2D depth integration of velocities and turbulence modelling and gives the domain of validity of the method.

Keywords ADV measurement · Fishway · Turbulence model · Shallow water · 2D modelling

1 Introduction

Flow around large-scale roughness, in which the size of bed elements has the same order of magnitude as the depth of flow, is of great interest, particularly for fish passage technology. So, modelling such complex 3D free surface flows using an industrial 2D code solving Saint Venant equations may appear at first as a challenge. Nevertheless, due to the complex setting-up and to excessive CPU time consumed by 3D free surface codes, the interest for a

✉ Ludovic Cassan
lcassan@imft.fr

[1] Water Ressources University, 175 Tay Son, Dong Da Dist, Hanoi, Vietnam

[2] Institut de Mécanique des Fluides de Toulouse, allée du Prof. Camille Soula, 31400 Toulouse, France

2D Saint Venant code remains timely. A similar approach using a 2D depth integrated model with comparison to measurements performed at Pprime Institute (Poitiers) was made by [7] with vertical slot fishways (VSF). Different from nature-like fishways (NLF), VSF consist of a sequence of pools connected by narrow vertical slots [8, 23, 24, 29]. To protect fish from unsuitable velocities, the total hydraulic head is divided into limited waterfalls localized at each slot, the water drop equalling the product of the longitudinal slope times pool length. [7] showed that the results of such numerical modelling were satisfactory as long as the longitudinal bottom slope does not exceed 10 % and excepted local zones having an appreciable vertical velocity component (plunging jet at slot passage).

Flow through NLF can be sketched as a free surface flow across an array of more or less arranged obstacles. Such flows generate great complication because they associate separation flow effects around obstacles with wakes interactions and possible transcritical zones. A dominant characteristic of such free surface flows is a strong agitation level and diphasic zones particularly for large longitudinal slope values. Instabilities are often observed along the wakes. So, the 3D nature of such flows appears as dominant (interactive wakes, horse shoe vortex) and they were investigated by many authors experimentally [11, 19, 21, 33] and numerically [15, 18, 28, 30, 32]. 3D industrial free surface codes do exist nowadays (MIKE3D, FLOW3D, STARCCM+, FLUENT...) but an efficient modelling necessitates using very big adaptive meshes and so CPU time consuming. Also, volume of fluids method, due to small cell sizes to capture free surface deformation, drastically increases the CPU time. So, the hydraulic engineer having a limited time to test several configurations and design an efficient nature-like fishway will be interested using a 2D shallow water industrial code like TELEMAC-2D.Nevertheless, the modeller has to be aware of the limitations due to underlying assumptions and hypotheses, such as hydrostatic pressure distribution and moreover due to the intrinsic nature of the flows under consideration.

The purpose of this paper is then to determine the ability of a 2D code to model flow through NLF and its limitations. We shall describe at first the experimental setup and the configurations tested. Then, the numerical model description and its procedure are given. The 2D depth averaged shallow water equations are solved using the code TELEMAC-2D. Turbulence closure uses the classical two equations $k - \epsilon$ closure model. In this paper, we focused about the cases of unsubmerged obstacles which appear more consistent with 2D depth averaged modelling. A comparison of computed water levels and velocities with measurements performed at the “Institut de Mécanique des Fluides de Toulouse” (IMFT), France, using optical methods and acoustic Doppler velocimetry, permitted to audit the numerical results. Turbulence modelling is necessary to fit the flow structure and, moreover, the turbulent kinetic energy is an important parameter to ensure suitable hydraulics for fish [22]. The validity of the $k - \epsilon$ closure model for a depth integrated 2D model is discussed for the present flow. Concerning the results, a special attention was paid to detect maximum velocity and turbulent kinetic energy. This last parameter is of great interest because its spatial distribution significantly affects the improvement relative to fish passage efficiency. Indeed the fishes have to find resting zones in the cylinders wakes to be able to pass the fishway by successive steps. Other parameters such as Reynolds shear stress and eddy size have been proven to be important in tests with some species [26, 27] but are not considered in this paper.

2 Experimental set up

Experimental laboratory results come from tests conducted in a tilting flume at the IMFT. The channel is 1 m wide and 7 m long, it is supplied by a centrifugal pump with a maximum discharge of 100 l/s. The roughness elements (wooden cylinders: diameter 12 cm − height 15 cm) have been regularly distributed at various concentrations C on a smooth or rough bottom. This last bottom corresponds to pebbles with sizes ranging from 30 to 50 mm. A previous experimental study [5] determined existing relationships between flow discharge and relative submersion for bottom slopes varying from 1 to 9 % and obstacles concentrations of 13 and 16 %. The concentration C is the ratio $D^2/a_x a_y$ where D is the diameter of cylinders, a_x and a_y are the distance between cylinder in the longitudinal and transversal directions respectively (see Fig. 1). Velocity profile measurements were performed using an acoustic doppler velocimeter (ADV) with a 3D probe giving the three velocity components at a sampling rate of 50 Hz, the (u, v, w) values corresponding to time-averaged measurements on 180 s. The averaged water depth h is obtained by shadowgraphy method using a 2K*2K video camera [5] and local water level measurements were made with a point gauge (precision 1 mm). The lateral averaged free surface position is measured with a frequency of 3 Hz. For each configuration, 600 pictures are averaged and integrated in the longitudinal direction to get the water depth. A configuration is defined by concentration C, discharge Q and slope S values. For each configuration an averaged velocity between cylinders, V_g, can be calculated with the following expression [5]. In the present paper measurements are only compared to numerical results for the configurations corresponding to unsubmerged obstacles (Table 1). In this table, P refers to the energy dissipation rate per unit volume which is commonly used for design and calculated as $P = \dfrac{\rho g Q S a_y}{a_x a_y h} = \dfrac{\rho g V_0 h a_x S a_y}{h} = \rho g S V_0$.

$$\frac{V_g}{V_0} = \frac{1}{1 - \sqrt{\frac{a_y}{a_x} C}} \tag{1}$$

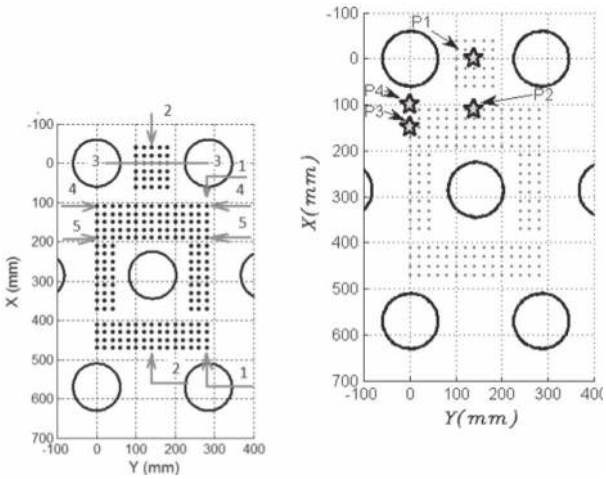

Fig. 1 Definition of lines used to plot results. Each black point represents the location of an ADV measurement. Stars markers (P1, P2, P3 and P4) indicate the location of vertical profiles

Table 1 Hydraulic conditions for ADV measurements

Exp	C (%)	Slope (S) (%)	Q (ls^{-1})	Bed	h(mm)	$V_g(ms^{-1})$	F	n (for 2D)($m^{-1/3}s$)	P (W/m^3)
E1	16	1	20	Rough	99	0.34	0.34	0.033	19.8
E2	16	2	40	Smooth	124	0.54	0.48	0.016	63.3
E3	16	3	50	Smooth	129	0.65	0.58	0.016	114.1
E4	16	5	50	Rough	110	0.76	0.73	0.033	222.9
E5	16	5	50	Smooth	100	0.83	0.83	0.016	245.2

with $V_0 = \dfrac{Q}{Bh}$ the bulk velocity.

We defined the experimental velocity magnitude as: $V = \sqrt{u^2 + v^2 + w^2}$

In order to characterize the flow pattern around a cylinder, the Froude number is based on V_g ($F = V_g/\sqrt{gh}$) [5].

The measurement zone corresponds to a flow equilibrium between gravity and dissipation. The velocity is measured 3 cm above the bed—Note that for rough cases, the bottom level depth origin is located above the stones crests. The measurement vertical position is imposed by ADV downlooking probe and by the distance between the probe and the measurement cell (5 cm).

3 Numerical modelling

3.1 Phenomena modelling

TELEMAC-2D [9, 12, 14, 20] provides hydrodynamic variables such as flow depth (h), depth-integrated velocity components (u, v) along X and Y directions, and turbulent kinetic energy (k) at every node of an unstructured triangular mesh. It solves continuity and momentum Saint Venant equations expressed in a non-conservative form using the finite element method. The intrinsic limitations of this code reside in the shallow water hypotheses and mainly on hydrostatic pressure distribution assumption and vertical component of velocity vector having a minor order of magnitude relative to horizontal ones. Turbulence modelling is obtained through classical $k - \epsilon$ closure model in its depth-integrated form [25], the pertinence of which will be discussed.

3.2 Model description

The model reproduces at full scale the geometry of the flume used during the experimental part of the study: length 7 m, width 1 m . The various patterns of unsubmerged circular cylinders for tested concentrations correspond to internal solid walls. The bottom was modelled as a friction zone parameterized by a Manning coefficient: $n = 0.0167\ m^{-1/3}s$ for smooth and $n = 0.0333\ m^{-1/3}s$ or $0.10\ m^{-1/3}s$ in order to represent the pebbles effects. The flow is computed for $C = 6$, 9, 13, 18 and 23 %, $Q = 10$, 20, 30, 40, 50, 70 and 90 l/s, $S = 1$, 2, 3, 4, 5, 6, 7, 8 and 9 %. For $C = 6$ and 9 %, the wake is unsteady, then the values are averaged over 30 s. All these simulations are performed to obtain the stage-discharge relationship of the fish pass for a given configuration.

3.3 The mesh

The 2D triangular unstructured grid must not have a too coarse mesh size particularly around cylinders where large flow depths deviations and intense velocity gradients occur. Several mesh size distributions were tested including large density around cylinders and coarser elsewhere. After several tests, the preferred grid size, offering the optimum ratio between quality of results and computing time, was a grid of size elements d with 9 mm $\leq$ d $\leq$ 30 mm, hereafter named 'standard' grid. For this grid, the total number of nodes used to model the geometries varies from about 19,500 to 21,000, depending on plots concentration value (see Fig. 2). So, a relative coarse meshing was chosen to build the 'standard' grids used to run the numerous simulations cases. In section 'velocity distribution', we shall discuss what improvement on water depth, velocities, turbulent kinetic energy would be expected using a 'fine' grid having a high nodes uniform density with about 830,000 nodes and cell size d: 1 mm $\leq$ d $\leq$ 5 mm (about 9 h of CPU time with 8 parallel processors).

3.4 Initial and boundary conditions

The boundary conditions used were a prescribed constant discharge at the model inlet and a depth-discharge relation at the outlet, with values corresponding to the experimental settings. At each time step, the outflow was calculated hereafter from the depth values at the outlet nodes using a rating curve relation issued from IMFT measurements [5].The outlet velocity distribution was considered as uniform. It must be noted that, due to blocking effect of the plots rows, the downstream boundary condition has no significant influence on the measurement zone corresponding to a flow equilibrium between gravity and dissipation. Concerning the wall velocity boundary condition, applied to lateral sides but also cylinders contours, the usual adherence condition leads to use a very dense mesh. Following [4, 10] who suggest to apply a weak wall condition, a free slip condition was imposed to velocity. For 2D depth-integrated equations, it must be verified that bottom friction is dominant relative to lateral wall friction. The best way to test validity of this weak condition is to verify that computed flow depths fit with experiments. The given results are relative to a gravity-dissipation equilibrium flow zone, the same as for measurements.

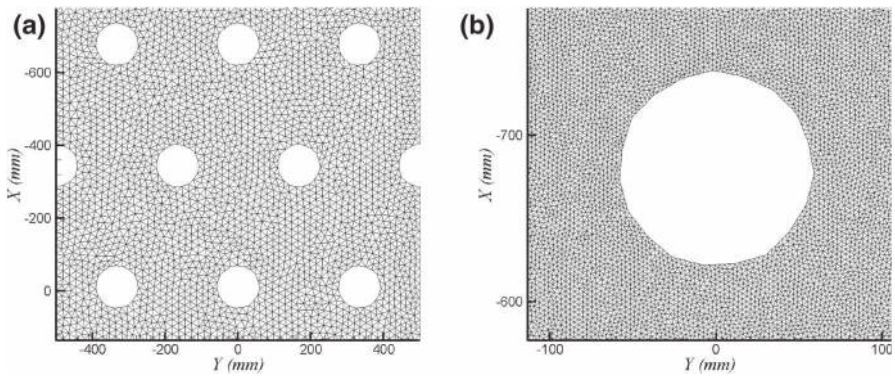

Fig. 2 Local view of the 'standard' (**a**) and 'fine' (**b**) grids

4 Results

4.1 Water surface elevation

The water surface elevation is measured along section 1-1 (see Fig. 3) for the hydraulic conditions with $C = 13$ %. The water profile is reproduced quite well by the 2D model up to a slope equal to 5 %. At steeper slope, the presence of a dry zone in the wake can explain significant local differences even if the mean water depth is estimated reasonably well by the model. The water elevation at the upstream side of cylinder is also under estimated by the fact that model assumptions are clearly not verified *i.e* the pressure is not hydrostatic and the velocity is strongly disturbed.

Fine mesh does afford a substantial improvement relative to standard mesh results (see Fig. 4). Although computed water depths for the case $C = 13$ %, $S = 5$ %, $Q = 50$ l/s still differ from measurements points at upstream (stagnation zone at points 4–8) and downstream (wake) vicinity of cylinders as an intrinsic limitation due to 2D modelling, a significant improvement is observed at the contraction zone between two rows of cylinders (points 1–11) and mainly into accelerated zone (points 2–10). This result is important for fish passage as it permits to better predict hydrodynamic zones having smaller depths and so higher velocities. But it must be emphasized that the presented case corresponds to the

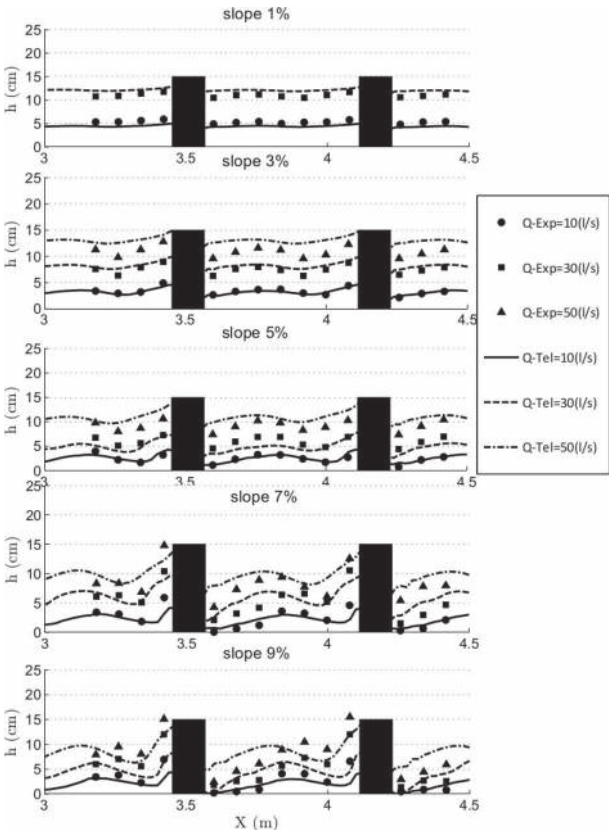

Fig. 3 Water surface profiles along section 1-1, for *C*=13 % and smooth bed

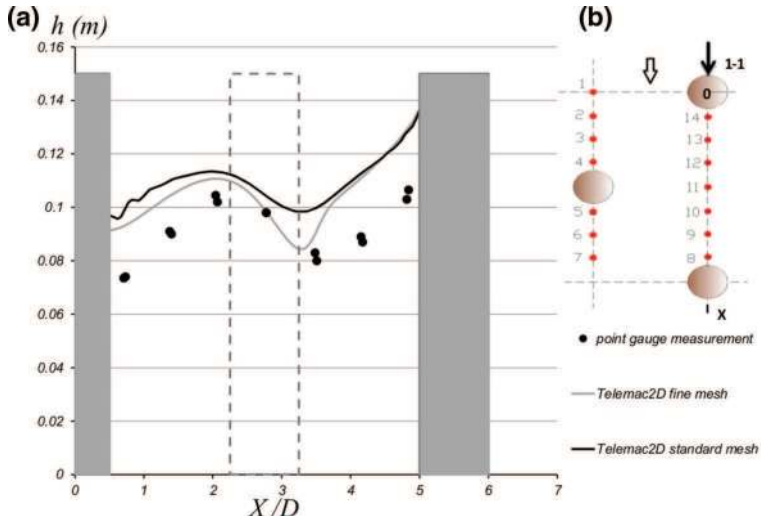

Fig. 4 **a** Water surface profiles along section 1-1 with fine and standard meshes and **b** diagram of measurement points

largest Froude number for this concentration. For smaller Froude, the free surface deformation is lower, then the difference between 2 meshes is reduced.

4.2 Velocity distribution

Velocities u are measured along vertical profiles with $C = 16$ % and smooth bed cases at 4 points as illustrated in Fig 1. Point P1 lies in the contracted zone located between 2 cylinders, point P2 lies in the âĂIJacceleration zoneâĂİ, points P3 and P4 are located in the downstream of the cylinder. These are the 4 points for which the depth- integrated modelling showed limitation in the simulation (especially in the case of great discharge and slope greater than 5 %). However at the points P1, P3 and P4, there is a relative agreement between the velocity u measured in experimental data and TELEMAC-2D. Figure 5

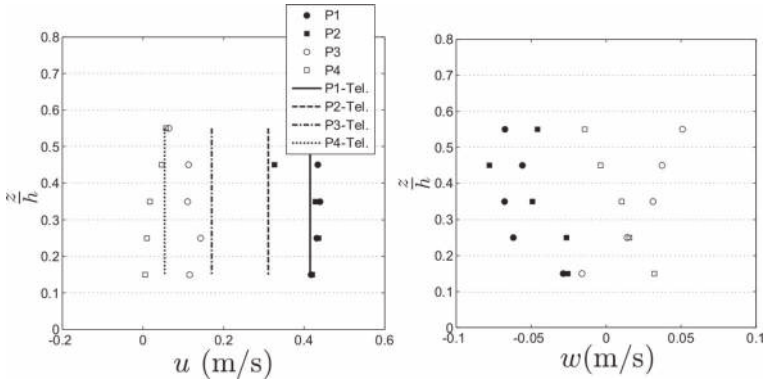

Fig. 5 Vertical velocity distribution for C = 16 %, S = 3 % and Q = 40 l/s and smooth bed. **a** Velocity component along X direction and **b** velocity component along Y direction

showed that the vertical velocity is distributed quite uniformly with deviations for low z/h values behind each cylinder; hence, the use of vertically integrated TELEMAC-2D modelling to simulate the nature-like fishway is suitable, except for low z/h values behind each cylinder. The vertical velocity w at the 2 points P1 and P2 has a negative value (see Fig. 5b) due to the contraction along the z axis and horizontal expansion in the flow in this zone. The water surface slope in this zone is great (plunging jet). The velocity profile at P3 and P4 are consistant with the recirculating zone identified by [1] behind a single cylinder. Vertical velocities are directed upward at the end of resting zone and they are equal to 15 % to the velocity between cylinder. Influence of this velocity on the fish rest has to be analysed in further studies to validate the passability. Nevertheless we will see that the 2D modelling of this zone is satisfactory for the most part.

The experimental velocity magnitude V is compared to simulations on the Fig. 6. The horizontal velocity distribution is considered in 4 sections 1-1; 3-3; 4-4 and 5-5 as shown in Fig. 1, sufficient to evaluate the velocity of critical points. The velocities are normalized using the averaged velocity value between cylinder given by (Eq. 1). As a consequence, the simulated velocity does not reach unity value because, as described in previous section, the computed water depth is over estimated. However the Fig. 6 shows that the horizontal velocities between TELEMAC-2D and ADV data are in good agreement. In the region between two cylinders, the variations of TELEMAC-2D and ADV values are very close with relative small deviation. The major discrepancies appear at points located in deceleration (upstream part of plots) and wake zones. The TELEMAC-2D velocity value decreases significantly when entering the deceleration zones (points where X/D = 3.8) and vice versa, the ADV value decreases significantly in the wake zones at X/D = 0.9 or Y/D = 0 and 2.3. In these areas, the distribution of velocity u along vertical is not uniform and velocity component w increases, hence, the limitation of the depth integrated model versus measurement data becomes much clearer compared to the ADV 3D measurement data.

Along section 1-1, it can be seen that: the maximum velocity V_{max} occurs in the range of X/D = 2.8 to 3.2. Due to the attachment of the flow around the cylinder, the velocity V_{max} is

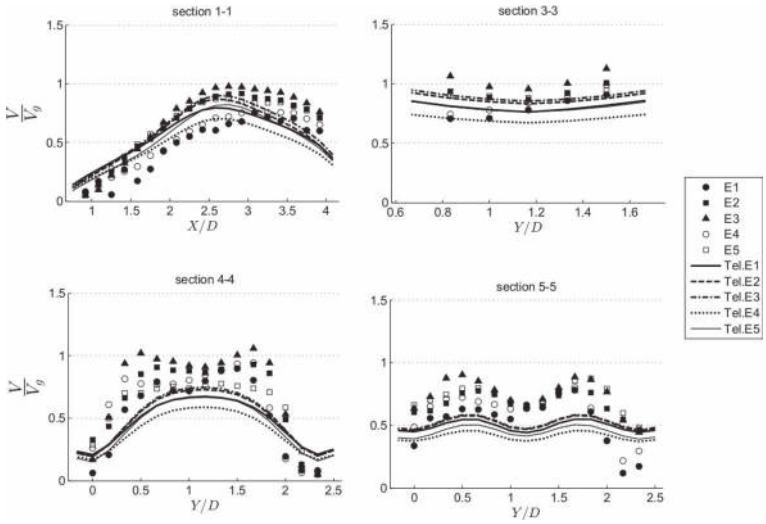

Fig. 6 Velocity magnitude in section 1-1, section 3-3, section 4-4 and section 5-5

also found at points Y/D = 0.8 and 1.5 (section 3-3). While the ADV maximum velocity is also found at the two points above, the TELEMAC-2D velocity increased steadily and reached its maximum at point X/D = 2.8 (section 1-1).

The transverse distribution (sections 4-4 and 6-6) in the downstream cylinder also reveals an under estimation of the velocity which is probably due to both an over estimation of the water depth and the dissipation from the turbulence model. As far as the ability of fish to pass is concerned, the 2D model is quite sufficient since maximum velocity is one of the main criteria used for fishway design. Also, the velocity in the resting zone are better reproduced and proves that 2D modelling is pertinent to evaluate flow in this zone.

Velocity above the pebble bed is smaller than with a smooth bed, possibly due to the higher velocity gradient involved by rough flow. The vertical distribution becomes less uniform than smooth flow.

In order to test mesh density influence on velocities, ADV measurements versus computation results are successively compared with the 'standard' mesh and the 'fine' mesh. The longitudinal velocity component u along the Sect. 2 is given for the case C=16 %, S = 5 %, Q = 50 l/s on Fig. 7. This concentration and slope correspond to the upper limit of the validity range as explained further. It appears that the mesh density does not impact the results except that maximal velocity value at contraction zone between the two cylinders is nearer to measurement with fine mesh. The computed velocity decreasing at upstream part is much greater than measurements but similar for the two meshes. Downstream of the cylinder, similar values and order of magnitude are compatible with measurements in the wake. The error due to the mesh is then inferior to 10 % which is not significant for fish passage. Moreover the CPU computation time for fine mesh is not compatible for a design process.

4.3 Turbulent fields

Turbulent kinetic energy k is more sensitive to mesh density and results obtained for C=16 %, S = 5 % , Q = 50 *l/s* case with 'fine' mesh present a systematic higher turbulence level than those obtained with the 'standard' mesh (see Fig.7b). The measured peak (0.2 m^2s^{-2}) is not reproduced in all cases.

These comparisons show that increasing mesh density does not improve significantly the quality of numerical results and that the 2D modelling intrinsic limitations remain dominant. For example, the numerical model underestimates the turbulence kinetic energy

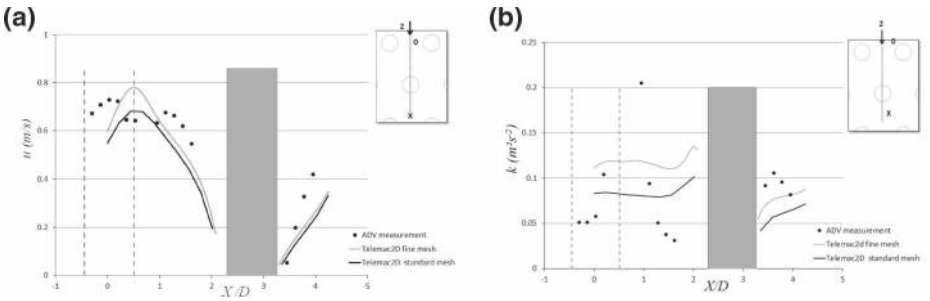

Fig. 7 Longitudinal velocity component **u** (**a**) and Turbulent kinetic energy **k** (**b**) along section 2-2: measurements and numerical results with two meshes

in the wake whereas the k is higher than experiments in front of the cylinder. However, the averaged value of k is reasonably reproduced between cylinder which allows to calculate a dissipation rate close to the experimental value and then reproduce the stage-discharge relationship (Fig. 8). Let us note that the turbulence peak for E5 experiment corresponds to an hydraulic jump which appears when the maximum Froude number becomes higher than 1 [5]. The magnitude of the turbulent kinetic energy is consistent with the experimental correlation from [2] even if the present measurements are weaker. The difference can be due to the fact that the dimensionless correlation are established for submerged conditions where the averaged velocity is relatively higher than for emergent conditions.

K-epsilon models permit to deal with complex flows and provide accurate solutions for a wide range of industrially relevant flows [17], its main default resides in misfitting for non-isotropic flow conditions or if strong instabilities develop. [6] tested three depth averaged turbulence models: mixing-length model (MLM), k-epsilon, and Algebraic Reynolds-Stress Model (ARSM) [25] and observed that the k-epsilon and ARSM models reproduced fairly well the size of recirculating regions. Nevertheless, problems can be located in flow zones with separation and reattachment zones along a short distance such as these encountered along cylinders and their wakes. K-epsilon model limitations are particularly due to Boussinesq hypothesis implying that Reynolds stresses are aligned with velocity gradient as expressed by the Reynolds stress expression

$$\overline{u_i' u_j'} = \frac{2}{3} k \delta_{ij} - 2 \nu_T S_{ij} \tag{2}$$

The eddy viscosity ν_T and the rate of strain tensor S_{ij} with i, j = indices corresponding to x,y components, u_i' = turbulent velocities fluctuations, k = turbulent kinetic energy and δ_{ij} = Kronecker symbol are given by

$$\nu_T = C_\mu \frac{k^2}{\varepsilon} \qquad (C_\mu = 0.09) \tag{3}$$

With ϵ = turbulent dissipation rate

$$S_{ij} = \frac{1}{2} \left(\frac{\partial u_i}{\partial x_j} + \frac{\partial u_j}{\partial x_i} \right) \tag{4}$$

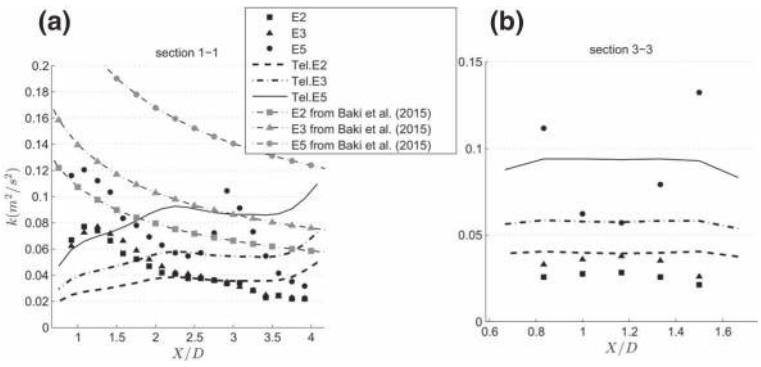

Fig. 8 Turbulent kinetic energy magnitude at **a** section 1-1 and **b** section 3-3

The anisotropy tensor defined by

$$a_{ij} = \frac{\overline{u_i' u_j'}}{k} - \frac{2}{3}\delta_{ij} \tag{5}$$

can be evaluated using Eq. (1) as

$$a_{ij} = -2\frac{v_T}{k}S_{ij} \tag{6}$$

The physical limitations are [31]

$$-\frac{2}{3} \leq a_{ij} < \frac{4}{3} \quad \text{for} \quad i = j \tag{7}$$

$$|a_{ij}| \leq 1 \quad \text{for} \quad i \neq j \tag{8}$$

In 2D depth-integrated cases, the three coefficients are

$$a_{11} = -2\frac{v_T}{k}\frac{\partial u}{\partial x} \tag{9}$$

$$a_{12} = -2\frac{v_T}{k}\frac{1}{2}\left(\frac{\partial u}{\partial y} + \frac{\partial v}{\partial x}\right) \tag{10}$$

$$a_{22} = -2\frac{v_T}{k}\frac{\partial v}{\partial y} = -a_{11} \tag{11}$$

The coefficients calculated from the results obtained with TELEMAC-2D k-epsilon modelling, show that the above-mentioned limits are respected, except at the upstream and downstream vicinity of the cylinders. So, the numerical results do not present elsewhere physically a priori unrealistic features (Fig. 9). This is not a sufficient proof of the model validity but a necessary one [16]. In fact we shall notice that water heights, velocity and kinetic turbulence energy field departures such as observed at the âĂIJnozzleâĂİ and wakes of the cylinders (in section 1-1) correspond to zones having a strong level of anisotropy. These zones also present typical 3D flow features such as horse-shoe vortices and noticeable vertical velocities which would only be resolved by 3D modelling, which is out of scope of our purpose which is to have a 2D efficient model knowing its limitations.

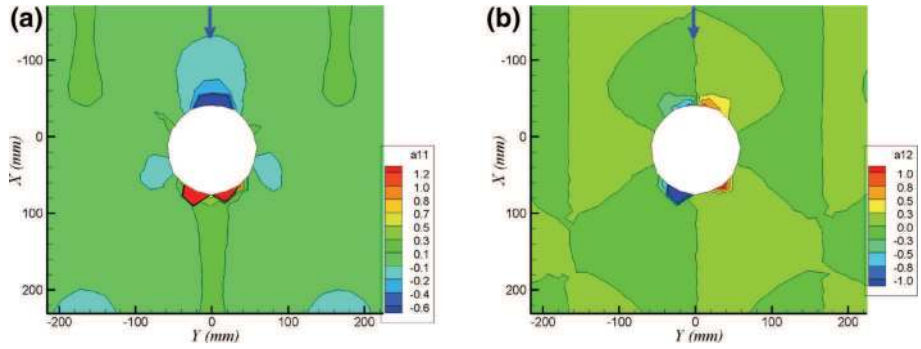

Fig. 9 Isotropy coefficients a_{11} **a** âĂŞ a_{12} **b** reveal limitation zones in *blue* or *red* colours

4.4 Stage-discharge relationship

In order to validate the 2D shallow water model in a large range of configurations ($6\,\% < C < 23\,\%$, $1\,\% < S < 9\,\%$), the simulations are compared to the experimental correlations from [5]. In this paper, the stage-discharge relationship is expressed with two coefficients which allows to separate bed and drag force. To this end, the momentum balance is written for the water volume in one cell around one cylinder (Eq. 12).

$$C_d \frac{Ch}{D} \frac{V_g^2}{gh} + (1 - \sigma C)\alpha C_f \frac{V_g^2}{gh} = 2S(1 - \sigma C) \tag{12}$$

Where α is the spatial correction coefficient, σ is the ratio between the cylinder area in the x, y plane and D^2, C_d is the drag coefficient and C_f is the bed friction coefficient. For the numerical results the value of C_f is computed by taking the averaged value of the bed shear stress provided by the calculation and depending on the Manning coefficient. The experimental measurement [5] allows to define the variation of the drag coefficient as a function of concentration, non-dimensional water depth ($h_* = h/D$) and Froude number, F.

$$C_d = C_{d0} f_C(C) f_F(F) f_{h_*}(h_*) \tag{13}$$

Where C_{d0} is the drag coefficient of a single, infinitely long cylinder with $F << 1$. The corrective function $f_C(C)$ is used to model the sheltering effect and $f_{h_*}(h_*)$ is needed to reproduce the bed influence on flow structure around the cylinder. The drag coefficient, C_d, resulting from simulation is calculated with Eq. 12, the inlet discharge and the averaged water depth on a cell. C_d values are depicted without corrective functions $f_{h_*}(h_*)$ and $f_C(C)$ in Fig. 10. It must be emphasized that $f_F(F)$ is not an experimental correlation but corresponds to the theoretical acceleration due to the vertical contraction and supercritical transition. Firstly, it can be observed that the bed friction and drag force are correctly separated by Eq. 12 since the same trend of C_d is observed for the three Manning coefficients. Unlike the experimental values, the numerical simulations are not corrected $f_{h_*}(h_*)$=1 and $f_C(C) = 1$. Nevertheless they have have similar trends as the function F from experiments. This fact appears logical since wake-bed interaction on flow structure is not taken into account by the 2D model. Similarly, the sheltering is not well reproduced but it has a little influence on discharge computation. When the flow transition occurs in the flow

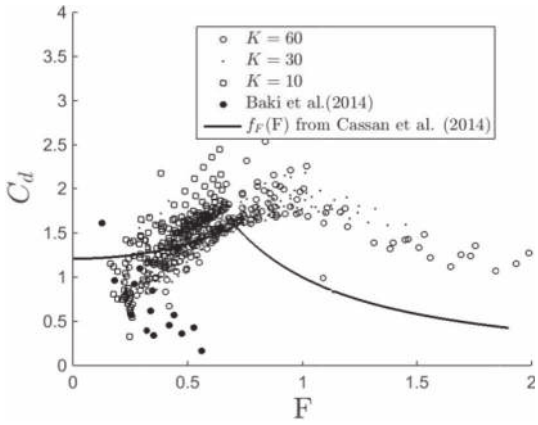

Fig. 10 Drag coefficient comparison between numerical values (*points*) and experimental correlation (*solid line*)

the velocity is near the critical value which explains the decrease of C_d as a function of F [5]. But this transition occurs for a lower F value in experiments than for simulation. Then the validity of 2D model is truly limited by the Froude number. The C_d extracted from experiments of [3] also presents a good agreement with the 2D model for the unsubmerged conditions. To obtain, the C_d value, the Eq. 12 is used. When the submerged conditions occurs the drag coefficient strongly decreases in comparison to the emergent case ($C_d < 0.9$ in Fig. 10).

The validity of 2D simulation is finally estimated by comparing the calculated discharge (Q_{model}) with experimental correlation (Q_{exp}) in the same configuration. For $F < 0.7$ (Fig. 11), the averaged error is 8 % and the standard deviation is equal to 15 %. To conclude, the 2D model provides a good approximation, albeit with a sizable deviation, of the stage discharge relationship for $F < 0.7$ which is the hydraulic condition of nature-like fish passes. The model user has to check if the Froude number calculated is in the validity range. Predictions of velocities and kinetic energy in certain areas only provide a first guess for passability estimation.

4.5 Implications for fish passage

The shallow water model has been used to define areas of low speed and low turbulence which can increase passage efficiency. The previous results show that the maximum velocity is located at the cylinder edge and can be estimated by V_g. The resting area can also be determined by focusing on zone where velocity is lower than a limit velocity depending on fish species. Herein the resting zone is defined by $V/V_g < a$ (where a can vary from 0.1 to 0.7) because the hydraulic condition are described independently of a specific fish species. These zones are in the cylinder wake, the width is almost equal to D and the length L depends mainly on the Froude number as shown on Fig. 12.

The zone is limited by the following cylinder rows which justifies that L is normalized by a_x. The Fig. 12 shows that L is less influenced by F in the range of validity ($F < 0.7$). This remark is confirmed by the ADV measurement. On the Fig. 6, the longitudinal profile of V/V_g is identical for all Froude number. This figure proves that the variation of L is linear as a function of a since $V/V_g \propto X/D$. As a consequence the resting area can be determined by simulation as a function of the criteria a and slightly corrected if $F > 0.6$.

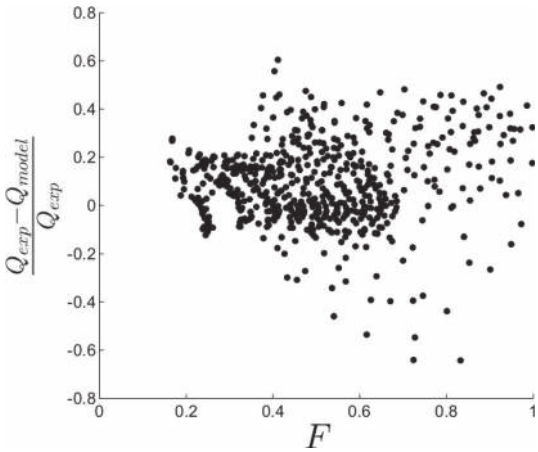

Fig. 11 Relative model discharge error

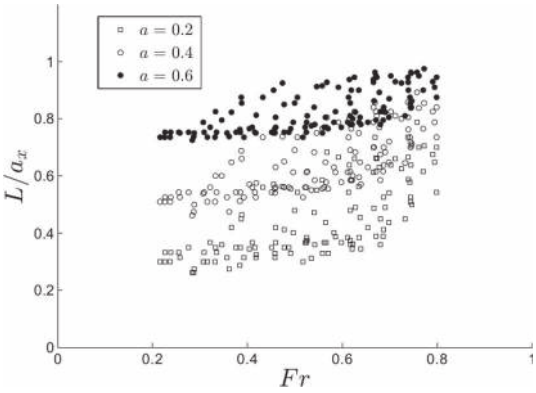

Fig. 12 Length of the resting zone as a function of the Froude number

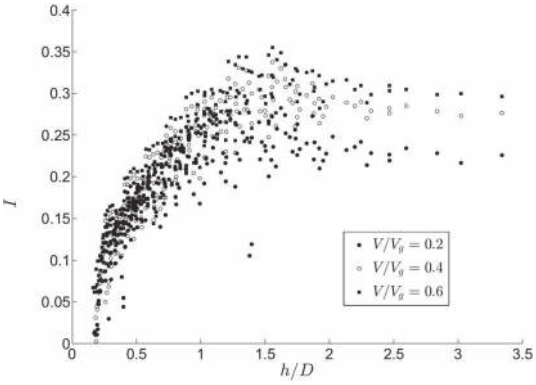

Fig. 13 Spatial averaged turbulent intensity in the resting zone as a function of the waterdepth

In order to confirm that this area is a possible resting zone, the spatial averaged k is calculated from simulations. The turbulent kinetic energy is normalized by the total kinetic energy between cylinder. The turbulent intensity is defined by:

$$I = \left(\frac{2}{3} \frac{k}{V_g^2} \right)^{(1/2)} \tag{14}$$

The turbulent intensity is depicted on Fig. 13 for simulation with an intermediate Manning coefficient ($n = 0.033\,\mathrm{m}^{-1/3}\,\mathrm{s}$). As the ADV measurements, the intensity is between 20 and 30 % for higher water depth depending on the criteria. When h/D is low, the turbulent energy is provided by the bed friction model whereas when h/D is higher, k tends to the value provided by the flow around cylinders. Between these two limits, the evolution is almost linear which allows to estimate a priori the turbulent energy. The ADV measurements are consistent with the simulation results even if the discrepancy can be explained by the vertical heterogeneity of k.

5 Conclusion

Velocity measurements in the nature-like fish passes represented by various surface piercing cylinders configurations have been performed in a large range of geometrical characteristics. A flow pattern has been identified and analyzed in order to study possible fish passage characteristics of this hydraulic structure. Considering the 3D free surface flow complexity such as encountered around obstacles, 2D modelling did not appeared at first as a fitting tool. Numerous shallow water simulations were performed in order to analyze if this 2D model can reproduce this particular free surface flow. A special attention was given to the turbulent model to explain discrepancy between experiments and numerical results. Finally, it was shown that a 2D depth integrated model can help the designer of the NLF. Indeed, in a specific range of slope ($S < 7$ %), cylinder concentration (6 % $< C <$ 20 %) and a Froude number less than 0.7, the numerical model provides maximum velocity and turbulent properties which are considered compatible with fish passage. As a consequence, the 2D model, which is quite easy to use, appears to be an available engineering tool for taking into account special geometrical configuration and adapting design to a fish species. 2D modeling should be used to investigate design options and lead to a more detailed examination (e.g. 3D modeling) of a final design for NLF.

References

1. Akilli H, Rockwell D (2002) Vortex formation from a cylinder in shallow water. Phys Fluids 14(9):2957–2967
2. Baki A, Zhu D, Rajaratnam N (2015) Turbulence characteristics in a rock-ramp-type fish pass. J Hydraul Eng 141(2):0733–9429
3. Baki A, Zhu D, Rajaratnam N (2014) Mean flow characteristics in a rock-ramp-type fish pass. J Hydraul Eng 140(2):156–168
4. Bazilevs Y, Michler C, Calo VM, Hughes TJR (2007) Weak Dirichlet boundary conditions for wall-bounded turbulent flows. Comput Methods Appl Mech Eng 196(49–52):4853–4862
5. Cassan L, Tien T, Courret D, Laurens P and Dartus D (2014). Hydraulic resistance of emergent macroroughness at large froude numbers: design of nature-like fishpasses. J Hydraul Eng 04014043
6. Cea L, Pena L, Puertas J, Vazquez-Cendon ME, Pena E (2007) Application of several depth-averaged turbulence models to simulate flow in vertical slot fishways. J Hydraul Eng 133(2):160–172
7. Chorda J, Maubourguet MM, Roux H, Larinier M, Tarrade L, David L (2010) Two-dimensional free surface flow numerical model for vertical slot fishways. J Hydraul Res 48(2):141–151
8. Clay CH (1995) Design of fishways and other fish facilities. CRC Press, London
9. Galland JC, Goutal N, Hervouet J-M (1991) TELEMAC-a new numerical-model for solving shallow-water equations. Adv Water Resour 14(3):138–148
10. Gorski JJ, Govindan TR, Lakshminarayana B (1985) Computation of three-dimensional turbulent shear flows in corners. AIAA J 23(5):685–692
11. Graf WH, Istiarto I (2002) Flow pattern in the scour hole around a cylinder. J Hydraul Res 40(1):13–20
12. Hervouet J-M (2007) Hydrodynamics of free surface flows: modelling with the finite element method. Wiley, Chichester
13. Hervouet J-M, Bates P (2000) The TELEMAC modelling system special issue. Hydrol Process 14(13):2207–2208
14. Hervouet JM (2000) The TELEMAC modelling system: an overview. Hydrol Process 14(13): 2209–2210
15. Hinterberger C, Froehlich J, Rodi W (2007) Three-dimensional and depth-averaged large-eddy simulations of some shallow water flows. J Hydraul Eng 133(8):857–872
16. Johansson A (2002). Engineering turbulence models and their development, with emphasis on explicit algebraic Reynolds stress models. Theories of Turbulence 442: 253–300
17. Jones RM, Harvey AD III, Acharya S (2001) Two-equation turbulence modeling for impeller stirred tanks. J Fluids Eng 123(3):640–648

18. Kawamura T, Mayer S, Garapon A, SÃűrensen L (2001) Large Eddy simulation of a flow past a free surface piercing circular cylinder. J Fluids Eng 124(1):91–101
19. Kirkil G, Constantinescu SG, Ettema R (2008) Coherent structures in the flow field around a circular cylinder with scour hole. J Hydraul Eng 134(5):587
20. Moulinec C, Hervouet J-M, Razafindrakoto E, Barber R, Emerson D and Gu X. TELEMAC, an efficient opensource HPC hydrodynamics suite. 22nd international conference on parallel computational fluid dynamics (ParCFD 2010)
21. Nepf HM, Sullivan JA, Zavistoski RA (1997) A model for diffusion within emergent vegetation. Am Soc Limnol Oceanogr 42(8):1735–1745
22. Odeh M, Noreika JF, Haro A, Maynard A, Castro-Santos T and Cada GF (2002). Evaluation of the effects of turbulence on the behavior of migratory fish. 2000-057-00, Report to Bonneville Power Administration, Portland
23. Rajaratnam N, Katopodis C, Solanki S (1992) New designs for vertical slot fishways. Can J Civ Eng 19(3):402–414
24. Rajaratnam N, Van der Vinne G, Katopodis C (1986) Hydraulics of vertical slot fishways. J Hydraul Eng 112(10):909–927
25. Rodi W (1984). Turbulence models and their applications in hydraulics, AIRH
26. Santos JM, Silva A, Katopodis C, Pinheiro P, Pinheiro A, Bochechas J, Ferreira MT (2012) Ecohydraulic approaches for restoring habitat connectivity and suitability. Ecol Eng 48:38–50
27. Silva A, Katopodis C, Santos JM, Ferreira MT, Pinheiro AN (2012) Cyprinid swimming behaviour in response to turbulent flow. Ecol Eng 44:314–328
28. Shao Wei-yun, Zhang Yi-ping, Zhu David Z, Zhang Tu-qiao (2013) Drag force on a free surface-piercing yawed circular cylinder in steady flow. J Fluids Struct 48:145–163
29. Tarrade L, Pineau G, Calluaud D, Texier A, David L, Larinier M (2011) Detailed experimental study of hydrodynamic turbulent flows generated in vertical slot fishways. Environ Fluid Mech 11(1):1–21
30. Tseng MH, Yen CL, Song CCS (2000) Computation of three-dimensional flow around square and circular piers. Int J Numer Methods Fluids 34(3):207–227
31. Wallin S, Johansson AV (2002) Modelling streamline curvature effects in explicit algebraic Reynolds stress turbulence models. Int J Heat Fluid Flow 23(5):721–730
32. Yu G, Avital EJ, Williams JJ (2008) Large eddy simulation of flow past free surface piercing circular cylinders. J Fluids Eng 130:101304–101304
33. Zhou Y, Zhang HJ, Yiu MW (2002) The turbulent wake of two side-by-side circular cylinders. J Fluid Mech 458:303–332